Journal of Vacuum Science & Technology A

The S_T component in the Si 2*p* photoemission spectrum from H-terminated and oxidized Si (001) surfaces

A. Herrera-Gomez, M.O. Vazquez-Lepe, P.G. Mani-Gonzalez, P. Pianetta, F.S. Aguirre-Tostado, O. Ceballos-Sanchez

CINVESTAV-Unidad Queretaro, Queretaro 76230, Mexico

Abstract

One doublet is usually employed to fit the Si^0 substrate species in the Si 2*p* photoemission spectra from Si (001) H-terminated (after piranha treatment) and oxidized surfaces. However, there is a second substrate-top component (S_T) with a binding energy 0.3 eV higher than the bulk component; its intensity varies from ~ 10% at normal emission (i.e., 90° from the surface) to ~ 20% at 35°. It is present even for oxidized surfaces and does not correspond to any of the suboxides species. It corresponds to the first layers of the substrate and is responsible for the decrease in the signal dip between the two S-O branches of the Si 2*p* spectra for glancing electron takeoff angles. Although it is resolvable for monochromatized sources, the S_T component is absent in the literature on Si 2*p* spectra.

I. Introduction

Because of its technological relevance, the Si 2*p* from the Si (001) surface is one of the most studied core levels with X-Ray Photoelectron Spectroscopy (XPS). The most common method for cleaning silicon wafers is Piranha [1], which produces a H-terminated hydrophobic silicon surface. This surface is widely used in silicon technology to grow silicon oxide or other materials to build semiconductor devices. There is extensive literature about the various peaks constituting the Si 2*p*

spectrum under different chemical environments. Synchrotron studies revealed the presence of various resolvable components in the Si^0 2*p* spectra for the atomically clean surface case [2–4]. Reports about the spectrum of H-terminated Si(001), either with synchrotron radiation or with laboratory equipment, are rare, if any. In the case of a thin silicon oxide on Si(001) analyzed with laboratory XPS equipment, the Si^0 2*p* component is usually fitted employing one doublet; in this paper, we show the presence a second resolvable component [5]. It does not correspond to any of the suboxide components discussed by Himpsel et al. [6] and others. We also show that the same extra component is also present in the Si 2*p* spectrum of H-terminated Si(001).

II. Experimental and analysis details

The samples employed were Si (001) n-type substrates. Except for one native silicon oxide sample (indicated in the text), all underwent RCA cleaning. This sulfuric acid/peroxide etch process, also known as "piranha", removes hydrocarbon residue; the HF last step removes the remaining oxide and yields a H-terminated surface.[1] The synchrotron experiments were carried out at (the old) Beamline 8-1 of the Stanford Synchrotron Radiation Laboratory with 130 and 260 eV light. Some of the RCA-processed samples were annealed at 850ºC for 10 min in the analysis chamber maintaining the pressure below 5×10^{-9} Torr; this provides atomically clean surfaces free of hydrogen [6].

The XPS laboratory data were acquired with an Intercovamex (Morelos, Mexico) assembled XPS instrument equipped with a hemispheric spectrometer (model XPS110) and an X-ray monochromator (model XR5) from ThermoFisher (East Grinstead, UK). The lens operation mode (MONOXPS) employed has an acceptance angle of 16°; the pass energy of the analyzer was set to 10 eV. The instrument broadening is approximately 0.4 eV under these conditions. Except for

one native-oxide sample, the Si(001) wafers underwent RCA cleaning. Four of the samples were thermally oxidized at 800 °C for 16, 26, 75, and 145 s; another sample was processed at 900 °C.

The peak analysis was carried out employing (real) Voigt singlets for O 1*s* and C 1*s* and doublets for Si 2*p*; for the latter, the ratio between the 1/2 and 3/2 components was fixed to the Scofield theoretical value for $h\nu$ = 130 eV (0.505, extrapolated from Reference [7]) and for Al Kα radiation (0.51, from Reference [8]). While the Lorentzian widths were fixed to previously known values (0.25 eV for O 1*s*, 0.35 eV for C 1*s*, 0.085 eV for Si^0 2*p* and 0.4 eV for Si^{4+} 2*p*), the Gaussian widths were allowed to vary during the optimization process. The background was modeled through the *Active Background Approach*, which allows for the simultaneous use of various background types to build the total background [9]. Another important analysis tool employed was the *Simultaneous Fitting Method* to robustly assess the peak parameters for data sets [10,11]. The uncertainties on the fitting parameters (areas, positions, and widths) were estimated through a rigorous approach (using the covariance matrix) that accounts for the covariance of the peak parameters with the background parameters [12] (in this way, the additional uncertainty on the peak intensities caused by the uncertainty on the background is accounted). The asymmetry was fitted with the *Double-Lorentzian* lineshape [13,14]. The peak fitting analysis was done with the software AAnalyzer® [15], which encompasses the analysis methods mentioned above.

The composition was calculated with the software XPSGeometry®, which is based on the *MultiLayer Model* (MLM) [16] The values employed for the differential cross-section [17] account for the partial polarization of the X-rays caused by the monochromator [18]. The effective attenuation lengths for each compound were calculated employing the Standard Reference Database 82 (EAL13) provided by NIST [19].

The angular analysis was done through the *Angular Transmission Function* approach described elsewhere [20], which allows for the modeling of the expected angular behavior once the physical model of the sample has been proposed. It allows for directly analyzing the peak intensities without normalizing the data at each angle to one of the components (usually, a bulk component). The reproduction of the intensity as a function of angle is achieved by accounting for the instrument-related geometrical factors affecting the intensity in XPS experiments (i.e., the angular transmission function).

III. Results

A. The S_T peak in the spectra from H-terminated Si (001) surfaces acquired with Al Kα radiation

The substrate feature of the Si 2*p* spectra from clean and oxidized Si (001) samples obtained with laboratory XPS equipment is usually fitted with one component. However, the presence of a surface component is strongly suggested by the decrease of the dip between the 1/2 and 3/2 spin-orbit branches for glancing angles, as shown in Figure 1.

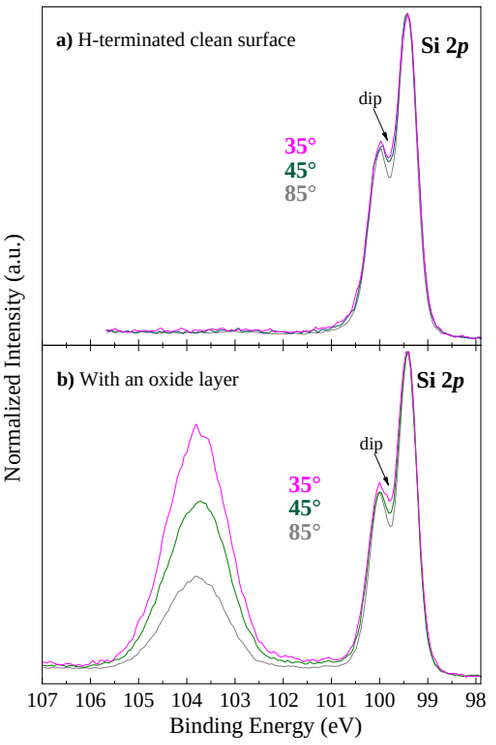

Figure 1. (Color online.) Si 2*p* spectrum at various electron take-off angles obtained with Al Kα (1,486.7 eV) monochromatized X-rays a) from an H-terminated Si (001) surface and b) from a SiO_2/Si (001) sample acquired at different angles. The decrease in the dip between the two S-O branches is indicative of the presence of a surface component around 99.7 eV.

The detection of this component can be hindered for several reasons. Some are illustrated in Figure 2, which shows different fitting scenarios for the 85° spectrum of the H-terminated sample also shown in Figure 1-a. It is an extended practice to peak-fit the XPS Si 2*p* feature from the substrate employing two independent singlets, one for the $2p_{3/2}$ and another for the $2p_{1/2}$ branch, as illustrated in Figure 2-a. The fit is good enough for most purposes. The small discrepancy between the experimental data and the fit around 100.4 eV is commonly overlooked or just ignored. Another issue that is also commonly overlooked is that the branching ratio (i.e., the intensity ratio of the 1/2 to the 3/2 branch) resulting from this fit is 0.55 instead of the qualitatively expected value of 0.5 or the theoretically predicted value of 0.51 [8]. When the branching ratio is forced to 0.51 (or to 0.5), the discrepancy in the fit appears in the two regions indicated by the dashed ovals in Figure 2-b. This double discrepancy suggests the presence of another peak, as

illustrated in Figure 2-c. This second peak, S_T (*substrate-top*), is shifted by about 0.3 eV to higher binding energy from the bulk component (*B*). The inset shows that the angular behavior of S_T is qualitatively different from that of the bulk signal; the blue and the black lines correspond to the expected behavior of a surface and a bulk component modeled through the *Angular Transmission Function* approach [20]. A thickness analysis, carried out under the MultiLayer Model using the discrete density approach,[16] shows that it corresponds to the top ~ 1.7 ML. (This analysis method is encompassed in the software XPSGeometry® [21].) Since its angular behavior is not substrate-like, it cannot be due to an alleged Si 2*p* peak asymmetry, as claimed in Reference [22] and illustrated in Figure 2-d. The fitting parameters employed for fits are displayed in Table I.

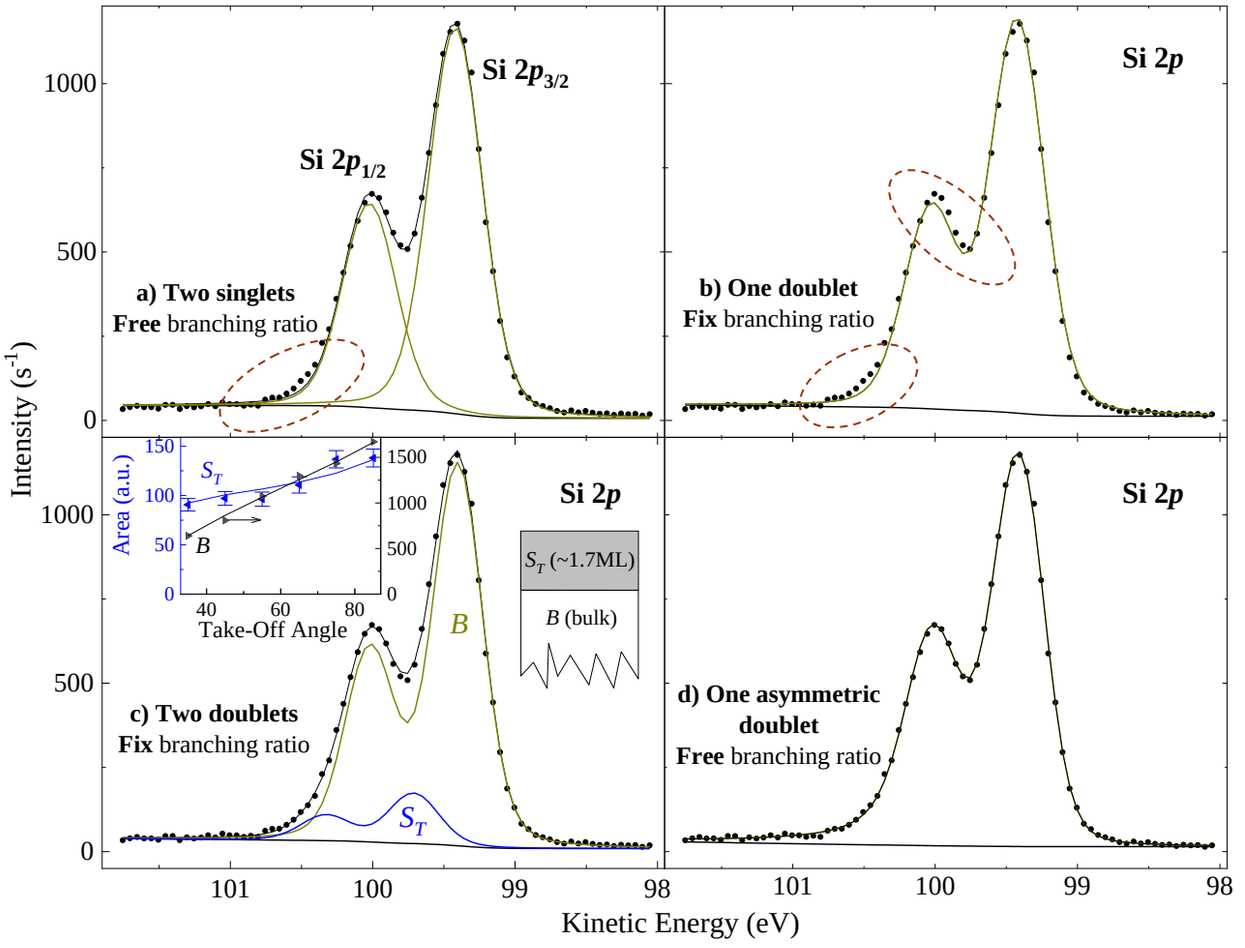

Figure 2. (Color online.) Si 2*p* spectrum from H-terminated silicon obtained with 1486.7 eV photons from a monochromatized Al Kα laboratory source. a) Fit employing two singlets, one for each branch. Besides a discrepancy in the fit around 100.5 eV, the branching ratio resulting from this procedure is 0.55 instead of the theoretical value of 0.51. b) Fit employing one double and forcing the branching ratio to 0.51. In this case, the discrepancy in the fit appears not only around 100.5 eV but also at 99.8 eV, on the top of the $2p_{1/2}$ branch. c) An appropriate fit can be obtained with two doublets, one corresponding to the bulk (*B*) and a second component (S_T) located 0.3 eV towards higher binding energy. The fit is excellent even though the branching ratio is forced to its theoretical value of 0.51 [8]. The inset shows that the angular dependency of S_T is different from the bulk component. d) The shape of the Si 2*p* spectrum has been attributed to an asymmetry [22]. Although the fit could be excellent by employing an asymmetric line-shape (double-Lorentzian[13]), it does not constitute a correct interpretation because of the different angular behavior of the *B* and S_T components shown in the inset of (c).

Table I. Parameters employed for the fits of the H-terminated Si 2*p* spectrum shown in Figure 2 a, b, c, and d. The background is a combination of SVSC and Slope backgrounds as described in Reference [9].

	Peak	$2p_{3/2}$ binding energy (eV)	Spin-orbit splitting (eV)	Gaussian width (eV)	Lorentzian width (eV)	Double Lorentzian Asymmetry
a)	bulk	99.4	0.6	0.36	0.085	n/a
b)	bulk	99.4	0.61	0.4	0.085	n/a
c)	bulk	99.4	0.61	0.37	0.085	n/a
	S_T	98.7	0.61	0.37	0.085	n/a
d)	bulk	99.4	0.61	0.36	0.081	2.32

B. The S_T peak in the spectra from SiO_2/Si (001) samples acquired with Al Kα radiation

The presence of S_T in the Si 2*p* spectrum from oxidized Si (001) surfaces acquired with laboratory Al Kα monochromatized source is also patent by the decrease on the dip between the two S-O branches for glancing angles, as illustrated in Figure 1-b. Figure 3 shows the fit (including S_T) of a Si 2*p* spectrum from a Si(001) substrate subjected to thermal oxidation at 800 °C for 75 s. Its angular dependence (inset) is qualitatively different from the bulk; it corresponds to a component at the top of the substrate (i.e., at the interface), which is consistent with the result shown in Figure 2-c. The thickness analysis, also carried out through the MultiLayer model employing the discrete density approach,[16] results in a value of ~ 2.0 ML for the layer corresponding to the S_T component. As for the clean sample, the blue and black lines of the inset, modeled employing the *Angular Transmission Function* approach [20] employing the physical model shown in Figure 3, are the expected behavior for substrate and interface components. It presented a small about of adventitious carbon due to its exposure to atmosphere during the transport from the oven to the XPS chamber. The parameters employed for these calculations are displayed in Table II.

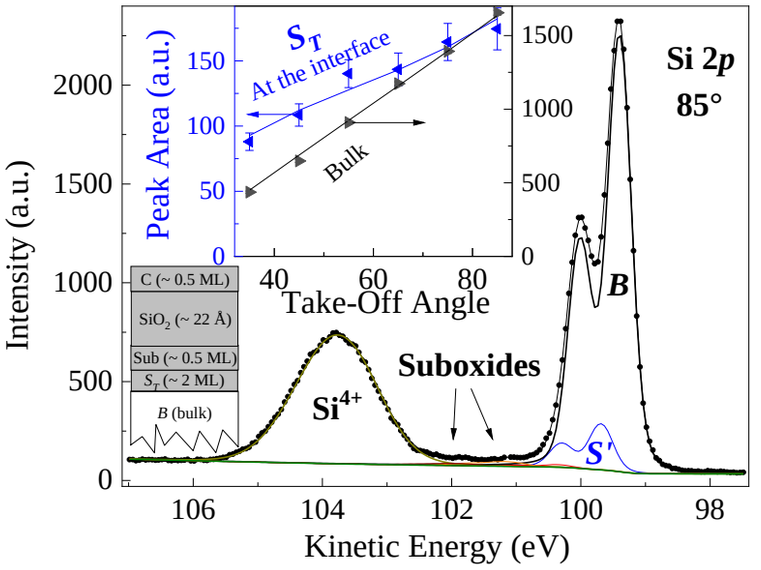

Figure 3. (Color online.) High-resolution spectrum of Si 2*p* for Si (001) with a thermal oxide layer (75 s at 800 °C in atmospheric pressure of ultra-high purity oxygen) approximately 6 Å thick. The S_T component is also required to fit the data. As in the data shown in Figure 5, there is a small number of suboxides ("Sub" in the diagram). The inset shows the angular dependence of S_T, strongly suggesting that this is a species located at the interface. The blue and black lines correspond to the expected angular behavior of an interface and a substrate component, respectively.

Table II. Parameters employed for the assessment of the thickness and composition of the samples. The differential cross sections and the effective attenuation lengths (EAL) were calculated using References [23] and [24], respectively.

Core level	$d\sigma/d\Omega$	EAL (Å)		
		Si	SiO_2	C
Si 2*p*	0.016784	29.86	35.08	33.54
O 1*s*	0.001878		23.49	25.12
C 1*s*	0.000641			27.93

C. Comparison with synchrotron data obtained with 130 and 260 eV photon energy

1. H-terminated surface

As discussed in Reference [25], the various components of the Si 2*p* spectrum for the clean Si (001) 2×1 surface have been characterized in detail. Synchrotron experiments, performed with a photon energy of 130 eV to minimize the effective attenuation length (~ 4 or 5 Å), clearly show the contribution to the photoelectron signal from each half of the outermost atomic monolayer and

also from the rest of the substrate [2]. The various components shown in Figure 4-a follow the nomenclature employed by Landemark et al. [2] In that work, *B* is associated with the bulk, which they define from the fourth monolayer on; *S* to the up-dimer atoms of the top surface monolayer (1/2 ML, shifted by +0.55 eV); *S'* to the second monolayer (shifted by -0.26 eV); *C* to the third monolayer (shifted by +0.3 eV). They resolved a fifth component between *B* and *S'*, called *SS* (shifted by -0.1 eV), which they assigned to the down dimers at the top surface. Notice that there is a small component corresponding to Si^{1+}. The interpretation of the physical origin of the various components is slightly different in the works of Pi et al. [3] and Gomoyunova et al. [4], although they all acknowledge their presence and that they are related to the first monolayers.

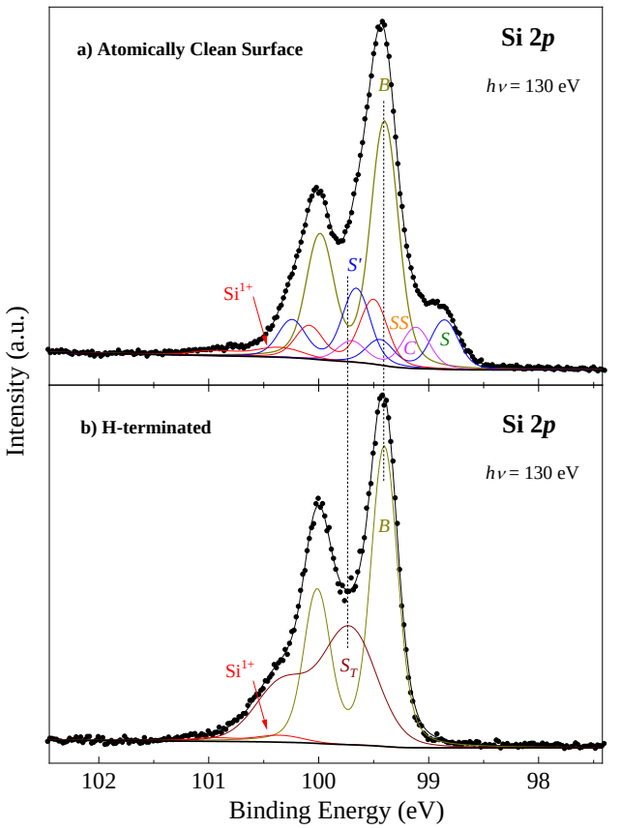

Figure 4. (Color online.) Si 2*p* spectra obtained with 130 eV photons a) from an atomically clean Si (001) 2×1 surface and b) from a H-terminated Si (001) 1×1 surface. The fit and terminology in (a) are similar to that proposed in Reference [2]. The S_T component in (b) is different from the Si^{1+} suboxide component. The relative intensity of S_T is approximately the same as the sum of the relative intensities of the *S*, *SS*, *C*, and *S'* components in (a).

For H-terminated Si (001) surfaces, the symmetry is 1×1 suggesting the absence of surface reconstruction. As shown for the Si 2*p* spectrum acquired with *hv* = 130 eV shown in Figure 4-b, the components corresponding to the last ~ two monolayers (*S*, *SS*, *C*, and *S'*) shift from their 2×1 corresponding binding energies and are comprised into a component with a BE ~ 0.3 eV above the bulk (i.e., at ~ BE = 99.7 eV). Its relative intensity (~ 42%) is approximately the same as the sum of the relative intensities of the *S*, *SS*, *C*, and *S'* components (~ 46%). The depth analysis shows that it corresponds to ~ the last two monolayers. For this analysis, it is necessary to use the *discrete approach* described in Reference [16] because the effective attenuation length is not much larger

than the Si (001) layer thickness. Except for being wider, it has all the important features (binding energy and depth profile) of the S_T component shown in Figure 2-c. The same results were found for data acquired with $h\nu$ = 260 eV light (not shown).

The presence of the same S_T component in both H-terminated Si (001) surface and SiO_2-covered surface suggests that the reconstruction of the top Si^0 layer is similar.

2. SiO_2/Si (001) sample

The presence of S_T in the SiO_2/Si (001) Si 2*p* spectra acquired with Al Kα radiation is also suggested by the decrease of the dip between the substrate's 1/2 and 3/2 spin-orbit branches, as shown in Figure 1-b. The Si 2*p* spectrum for the oxidized Si (001) surface has also been characterized in detail. By using synchrotron radiation with $h\nu$ = 130 eV, Himpsel et al. characterized the shift and FWHM of the oxide and suboxide peaks (Si^{4+}: shift 3.9 eV, FWHM 1.15 eV; Si^{3+}: shift 2.5 eV, FWHM 0.7 eV; Si^{2+}: shift 1.75 eV, FWHM 0.6 eV; Si^{1+}: shift 0.95 eV, FWHM 0.44 eV) [26]. The fit shown in Figure 5, which corresponds to a native-oxide Si (001) sample acquired with 260 eV light, was done using Himpsel's peak parameters except for considering the extra component S_T. Then, besides the peaks associated with Si^{4+}, Si^{1+}, Si^{2+}, Si^{3+}, and Si^0 proposed by Himpsel et al., it is also necessary to consider S_T as the clean surface.

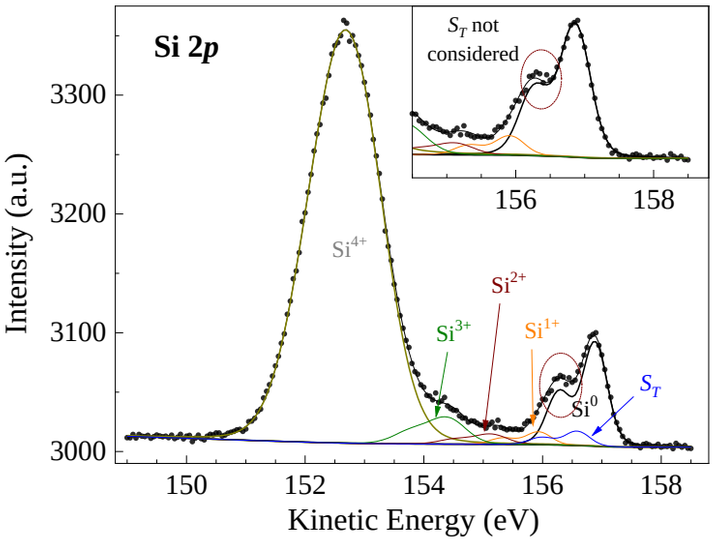

Figure 5. (Color online.) Si 2*p* spectrum obtained with 260 eV photons. The energy shift and Gaussian width of the peaks employed for the fit are those from Reference [26]. The extra component, S_T, was not considered in the series of works by Himpsel et al.[26] However, as shown in the inset, the fit is improved in the circled region by including S_T.

D. Comparison with previous work

Oh et al. [27], and later Dreiner et al. [28] and Owaga et al. [29], reported the presence of two extra Si 2*p* components, α and β, in the Si^0 region found from peak-fitting. We observed that our data was also possible to be fitted with those components, as illustrated in Figure 6-a. However, the fit requires only one extra component (S_T), i.e., although it is possible to use the β peak, it is not required to get a good fit (as shown in Figure 6-b). We prefer case (b) because it requires a smaller number of peaks, and the angular behavior of S_T is well behaved.

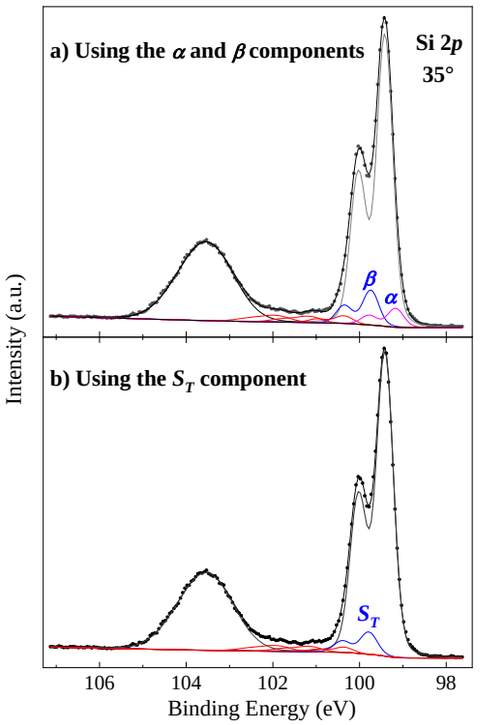

Figure 6. (Color online.) Fit of the Si 2p spectra from Si (001) annealed at 800 °C for 16 second; the data was acquired at 35° take-off angle (from the surface). a) Fit employing the α and β components proposed by Oh et al. [27]. b) Fit employing the S_T component proposed in this work. This shows that the component β is not required to obtain a good [16] fit.

E. Physical origin of the S_T component

It has been proposed that the α and β components correspond to chemical species at the interface with fix thickness.[27–30] This is inconsistent with our finding that the thickness of the ST layer varies with the thickness of the oxide layer. We analyzed the behavior of the S_T component from a series of samples consisting of thin silicon oxide layers on Si (001) substrates prepared under different conditions. Their structure, including the thickness of the S_T layer, the suboxides, and the SiO_2 layer, was assessed through the MultiLayer Model[16] from ARXPS data. As shown in Figure 7-a, except for the native-oxide sample, there seems to be a well-defined dependence of the Si^{4+} shift with the thickness of the layer associated to S_T. The exception of the native-oxide sample is corrected when the thickness of the oxide layer is accounted (Figure 7-b).

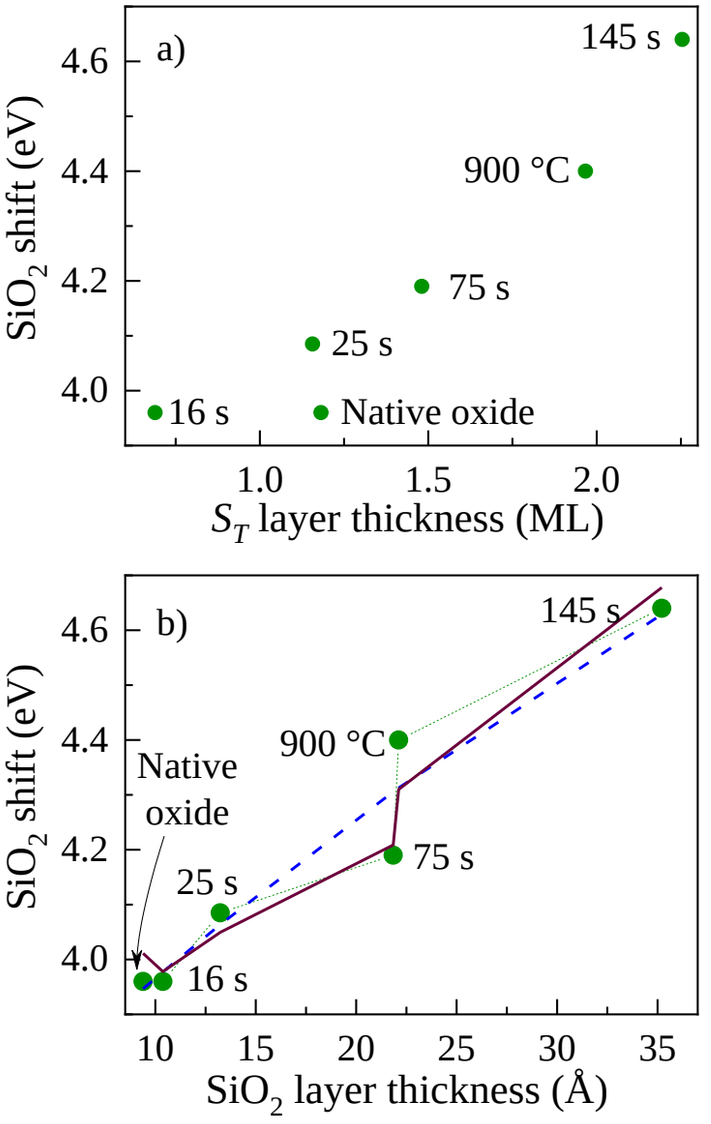

Figure 7. (Color online.) Correlation between the Si^{4+} shift and the thickness of the S_T layer. a) Dependence of the Si4+ shift and the thickness of the S_T layer. b) The blue dashed line corresponds to the fit in which it is considers that the surface charge is constant. The solid cardinal line corresponds the fit to the model presented in this paper (described in the text) in which the surface charge varies with the thickness of the S_T layer. In contrast with the constant layer model, our model reproduces the jump on the binding energy of the Si 2*p* peak in Si^{+4} between the 75 s and 900 °C samples.

As it has been reported elsewhere [31,32], the thicker the SiO_2 layer, the larger the shift of the Si 2*p* component associated to Si^{4+}. Kim et al. [32] showed that this dependence can be explained in terms of a positive charge at the oxide surface compensated with a negative charge at the interface (this is discussed at length in Reference [5]). To model the shift observed by the Si^{4+} component, they

consider that this surface charge is independent on the SiO_2 layer thickness. In their Eq. 3, they convolve the lineshape of the peak (assumed to be Gaussian) with a peak center varying with position, with the Beer-Lambert attenuation factor.

We employed a more precise approach to model the dependence of the shift of the silicon oxide component on its thickness. The change on the kinetic energy caused by the dipole layer on the substrate photoelectrons, δK_{sub}, is equal to $e\sigma d/\varepsilon$, where *e* is the electron charge (positive), σ is the surface charge density (positive), ε is the dielectric constant of SiO_2, and *d* is the SiO_2 layer thickness. The increment is positive because the field in the oxide layer is such that it accelerates the electrons. The change on the kinetic energy of the electrons from the oxide layer originated at depth *z* measured from the surface of the layer is

$$\delta K_{\mathrm{ox}}(z) = e\sigma z/\varepsilon, \qquad \text{Eq. 1}$$

also positive. Since the electrons closer to the surface contribute more to the signal, this change on the kinetic energy must be weighted by the Beer-Lambert attenuation factor as follows:

$$\overline{\delta K}_{\mathrm{ox}} = \frac{\int_0^d dz \frac{e\sigma z}{\varepsilon} \exp\left(-\frac{z}{\lambda \sin\theta}\right)}{\int_0^d dz \exp\left(-\frac{z}{\lambda \sin\theta}\right)} = \frac{e\sigma}{\varepsilon}\left[\lambda \sin\theta - \frac{d}{\exp\left(\frac{d}{\lambda \sin\theta}\right)-1}\right], \qquad \text{Eq. 2}$$

where λ is the effective attenuation length and θ is the photoemission take-off angle measured from the surface. This expression reduces to $e\sigma/\varepsilon\, d/2 \sin\theta$ for large λ, and to $e\sigma/\varepsilon\, \lambda \sin\theta$ for small λ, as expected. This total difference in binding energy between the Si 2*p* peak originated from the substrate and that originated in the oxide layer (ΔBE_{total}) is the sum of the chemical shift ($\Delta BE_{\mathrm{chem}}$) and the extra shift caused by the dipole field ($\Delta BE_{\mathrm{dipole}}$), where

$$\Delta BE_{\mathrm{dipole}} = \delta K_{\mathrm{sub}} - \overline{\delta K}_{\mathrm{ox}}, \qquad \text{Eq. 3}$$

resulting in

$$\Delta BE_{total} = \Delta BE_{\text{chem}} + \frac{e\sigma d}{\varepsilon} - \frac{e\sigma}{\varepsilon}\left[\lambda \sin\theta - \frac{d}{\exp\left(\frac{d}{\lambda \sin\theta}\right) - 1}\right]. \quad \text{Eq. 4}$$

The last term is always smaller than the second, so the change in the total shift is positive. This is because the electrons from the substrate are accelerated along the whole layer and are subjected to a larger kinetic energy shift than the oxide. Since the spectra is aligned to the Si 2*p* substrate peak (99.4 eV binding energy), the shift is only apparent in the oxide peak.

Figure 7-b shows the dependence of the Si^{4+} shift with the thickness of the oxide layer for the same samples. The dashed-blue line corresponds to a constant surface charge density, as considered in their model by Kim et al.[32] The cardinal-solid line corresponds to modeling σ as linearly dependent on the thickness of the S_T layer as follows:

$$\sigma = \sigma_0 + \sigma' d_{S_T} . \quad \text{Eq. 5}$$

The values for $\sigma_0 = 0$ and $\sigma' = 3.7\times10^{-4}\, e/\text{Å}^3$ correspond to the optimum fit to the experimental data (green dots). It is remarkable that considering the surface charge to be proportional to the *S'* layer thickness qualitatively reproduces the behavior of the Si^{4+} shift and that the optimal value for the constant term σ_0 is equal to zero. This strongly suggests that the S_T component is related to charge accumulation at the top of the substrate. Under this model, the corresponding accumulation charge per unit surface layer is 5×10^{-3} *e*. The value for ΔBE_{chem} is different between the two models: 3.63 eV for the constant σ model, and 3.92 eV for the model considering σ proportional to the thickness of the S_T layer.

Our conclusion is that the S_T component is due to negative charge accumulated at the Si\SiO$_2$ interface. This suggests that that the shift of S_T towards higher binding energy is due to a

perturbation caused by the interface charge on the electronic structure of the S_T atoms without affecting their total atomic charge.

In the case of the H-terminated surfaces, there is also a negative surface charge accumulated in response to the positive charge of the hydrogen atoms. It is very likely that, as in the H-terminated case, the presence of the thermal silicon oxide eliminates the reconstruction of the top Si substrate layer, as it is suggested by the lack of band bending in both cases (band bending is related to surface reconstruction, as shown in Figure 5 of Reference 33). In the same way as in the SiO_2/Si case, the S_T component might arise as an electronic state response to the presence of the surface states negative charge without the shift to higher binding energies representing loss of charge.

IV. Conclusions

The substrate feature in the photoemission spectrum of Si 2*p* from H-terminated Si (001) and SiO_2/Si (001) samples acquired with Al Kα radiation has a resolvable peak, which we call S_T, with binding energy ~ 0.3 eV above the Si^0 bulk peak. It is also found in H-terminated surfaces employing synchrotron photon energies (130 eV and 260 eV) that enhance the top surface contribution. Even though the Si 2*p* photoemission spectrum is one of the most studied, this component has been overlooked in the literature. Its presence causes a decrease in the dip between the two S-O components of the main Si^0 2*p* doublet for glancing electron take-off angles. It is relatively small, ~ 10% of the substrate peak at normal electron emission (90°), and ~ 20% at 35°. Its angular dependence is quantitatively described by a layer with a depth location at the top of the silicon substrate. It is present even for oxidized surfaces and does not correspond to any of the suboxide species.

The similarity of the Si^0 2*p* component of the H-terminated Si (001) 2×1 surface and of the SiO_2-covered surface suggest that the presence of the oxide eliminates the reconstruction of the substrate in the same way as hydrogen does.

Although it was suggested that the presence of similar components is associated with surface species with fixed thickness, the dependence of its thickness on the thickness of the SiO_2 layer discards that model. We found that the thickness of the S_T layer is governed by the dipole charge between the top surface oxide and the SiO_2/Si interface. In the same way, the shift of the Si^{+4} is governed by the strength of the dipole. In the case of H-terminated samples, the negative charge at the substrate surface is caused by the positively charged hydrogen atoms.

Acknowledgments

This work was supported in part by CONACyT Proyecto Fronteras 58518.

Data Availability

The data that support the findings of this study are available from the corresponding author upon reasonable request.

Conflict of interest

The authors have no conflicts to disclose.

References

[1] W. Kern, and D.A. Puotinen, RCA Rev. **186**, 187–206 (1970).

[2] E. Landemark, Y.C. Karlsson, and R.I.G. Uhrberg, PHYS REV LETT **69**, 1588 (1992).

[3] T.W. Pi, I.H. Hong, C.P. Cheng, and G.K. Wertheim, J ELECTRON SPECTROSC **107**, 163–176 (2001).

[4] M. V. Gomoyunova, and I.I. Pronin, Technical Physics **49**, 1249–1279 (2004).

[5] A. Herrera-Gómez, *An Extra Peak in the Si 2p XPS Spectrum*. Internal Report Cinvestav-Queretaro http://www.qro.cinvestav.mx/~aherrera/reportesInternos/extraPeakSi2p.pdf (2001).

[6] F.J. Himpsel, F.R. McFeely, A. Taleb-Ibrahimi, J.A. Yarmoff, and G. Hollinger, PHYSICAL REVIEW B **38**, 6084–6096 (1988).

[7] J.H. Scofield, *Theoretical Photoionization Cross Sections from 1 to 1500 KeV* (1973). doi:10.2172/4545040.

[8] J.H. Scofield, J ELECTRON SPECTROSC **8**, 129–137 (1976).

[9] A. Herrera-Gomez, M. Bravo-Sanchez, O. Ceballos-Sanchez, and M.O. Vazquez-Lepe, SURF INTERFACE ANAL **46**, 897–905 (2014).

[10] A. Herrera-Gomez, *Simultaneous data fitting in ARXPS*, I Internal Report Cinvestav-Queretaro, Mexico, http://Www.Qro.Cinvestav.Mx/~aanalyzer/SimultaneousFitting.Pdf (2008).

[11] J. Muñoz-Flores, and A. Herrera-Gomez, J ELECTRON SPECTROSC **184**, 533–541 (2012).

[12] A. Herrera-Gomez, J VAC SCI TECHNOL A **38**, 033211 (2020).

[13] A. Herrera-Gomez, *A Double Lorentzian Shape for Asymmetric Photoelectron Peaks*. Internal Report Cinvestav-Queretaro, Mexico, http://www.qro.cinvestav.mx/~aherrera/reportesInternos/doubleLorentzian.pdf (2011).

[14] G.H. Major, T.G. Avval, D.I. Patel, D. Shah, T. Roychowdhury, A.J. Barlow, P.J. Pigram, M. Greiner, V. Fernandez, A. Herrera-Gomez, and M.R. Linford, SURF INTERFACE ANAL **53** 689–707 (2021).

[15] A. Herrera-Gomez, "AAnalyzer®, a software for XPS-data peak-fitting," https://xpsoasis.org/aanalyzer_manual / (2000).

[16] A. Herrera-Gomez, *Self Consistent ARXPS Analysis for Multilayer Conformal Films with Abrupt Interfaces* Internal Report Cinvestav-Queretaro, Mexico. http://www.qro.cinvestav.mx/~aherrera/reportesInternos/arxpsAnalysisSharpIntefaces.pdf (2008).

[17] J.J. Yeh, and I. Lindau, Data Nucl Data Tables **32**, 1–155 (1985).

[18] A. Herrera-Gomez, J ELECTRON SPECTROSC **182**, 81–83 (2010).

[19] C.J. Powell, and A. Jablonski, "NIST Standard Reference Database 82 NIST Electron Effective-Attenuation-Length Database," (2011).

[20] A. Herrera-Gomez, F.S.S. Aguirre-Tostado, P.G.G. Mani-Gonzalez, M. Vazquez-Lepe, A. Sanchez-Martinez, O. Ceballos-Sanchez, R.M.M. Wallace, G. Conti, and Y. Uritsky, J ELECTRON SPECTROSC **184**, 487–500 (2011).

[21] A. Herrera-Gomez, *XPSGeometry, a software for the analysis of ARXPS data*. http://qro.cinvestav.mx/~aherrera/web/software.htm (2007).

[22] D.F. Mitchell, K.B. Clark, J.A. Bardwell, W.N. Lennard, G.R. Massoumi, and I. V Mitchell, SURF INTERFACE ANAL **21**, 44–50 (1994).

[23] A. Herrera-Gomez, J ELECTRON SPECTROSC **182**, 81–83 (2010).

[24] C.J. Powell, and A. Jablonski, *NIST Electron Effective-Attenuation-Length Database Version 1.3* (National Institute of Standards and Technology, Gaithersburg, Maryland, 2011).

[25] A. Herrera-Gomez, F.-S. Aguirre-Tostado, and P. Pianetta, J VAC SCI TECHNOL A **34**, 020601 (2016).

[26] F.J. Himpsel, P. Heimann, T.C. Chiang, and D.E. Eastman, PHYS REV LETT **45**, 1112–1115 (1980).

[27] J.H. Oh, H.W. Yeom, Y. Hagimoto, K. Ono, M. Oshima, N. Hirashita, M. Nywa, A. Toriumi, and A. Kakizaki, PHYSICAL REVIEW B **63**, (2001).

[28] S. Dreiner, M. Schürmann, M. Krause, U. Berges, and C. Westphal, J ELECTRON SPECTROSC **144-147**, 405–408 (2005)

[29] S. Ogawa, J. Tang, A. Yoshigoe, S. Ishidzuka, and Y. Takakuwa, J. Chem. Phys. **145**, (2016).

[30] O. V. Yazyev, and A. Pasquarello, PHYS REV LETT **96**, (2006).

[31] T. Eickhoff, V. Medicherla, and W. Drube, J ELECTRON SPECTROSC **137–140**, 85–88 (2004).

[32] W.B. Kim, M. Nishiyama, and H. Kobayashi, J ELECTRON SPECTROSC **176**, 8–12 (2010).

[33] A. Herrera-Gómez, F.S. Aguirre-Tostado, Y. Sun, P. Pianetta, Z. Yu, D. Marshall, R. Droopad, and W.E. Spicer, J Appl Phys **90**, 6070–6072 (2001).

Tables

Table I. Parameters employed for the fits of the H-terminated Si 2p spectrum shown in Figure 2 a, b, c, and d. The background is a combination of SVSC and Slope backgrounds as described in Reference 9.

	Peak	$2p_{3/2}$ binding energy (eV)	Spin-orbit splitting (eV)	Gaussian width (eV)	Lorentzian width (eV)	Double Lorentzian Asymmetry
a)	bulk	99.4	0.6	0.36	0.085	n/a
b)	bulk	99.4	0.61	0.4	0.085	n/a
c)	bulk	99.4	0.61	0.37	0.085	n/a
	S_T	98.7	0.61	0.37	0.085	n/a
d)	bulk	99.4	0.61	0.36	0.081	2.32

Table II. Parameters employed for the assessment of the thickness and composition of the samples. The differential cross sections and the effective attenuation lengths (EAL) were calculated using References [23] and [24], respectively.

Core level	$d\sigma/d\Omega$	EAL (Å)		
		Si	SiO_2	C
Si 2*p*	0.016784	29.86	35.08	33.54
O 1*s*	0.001878		23.49	25.12
C 1*s*	0.000641			27.93

Figure Captions

Figure 1. (Color online.) Si 2*p* spectrum at various electron take-off angles obtained with Al Kα (1,486.7 eV) monochromatized X-rays a) from an H-terminated Si (001) surface and b) from a SiO2/Si (001) sample acquired at different angles. The decrease in the dip between the two S-O branches is indicative of the presence of a surface component around 99.7 eV.

Figure 2. (Color online.) Si 2*p* spectrum from H-terminated silicon obtained with 1486.7 eV photons from a monochromatized Al Kα laboratory source. a) Fit employing two singlets, one for each branch. Besides a discrepancy in the fit around 100.5 eV, the branching ratio resulting from this procedure is 0.55 instead of the theoretical value of 0.51. b) Fit employing one double and forcing the branching ratio to 0.51. In this case, the discrepancy in the fit appears not only around 100.5 eV but also at 99.8 eV, on the top of the 2p1/2 branch. c) An appropriate fit can be obtained with two doublets, one corresponding to the bulk (B) and a second component (ST) located 0.3 eV towards higher binding energy. The fit is excellent even though the branching ratio is forced to its theoretical value of 0.51 8. The inset shows that the angular dependency of S_T is different from the bulk component. d) The shape of the Si 2*p* spectrum has been attributed to an asymmetry 23. Although the fit could be excellent by employing an asymmetric line-shape (double-Lorentzian 24), it does not constitute a correct interpretation because of the different angular behavior of the *B* and S_T components shown in the inset of (c).

Figure 3. (Color online.) High-resolution spectrum of Si 2*p* for Si (001) with a thermal oxide layer (75 s at 800 °C in atmospheric pressure of ultra-high purity oxygen) approximately 6 Å thick. The S_T component is also required to fit the data. As in the data shown in Figure 5, there is a small number of suboxides ("Sub" in the diagram). The inset shows the angular dependence of S_T, strongly suggesting that this is a species located at the interface. The blue and black lines correspond to the expected angular behavior of an interface and a substrate component, respectively.

Figure 4. (Color online.) Si 2*p* spectra obtained with 130 eV photons a) from an atomically clean Si (001) 2×1 surface and b) from a H-terminated Si (001) 1×1 surface. The fit and terminology in (a) are similar to that proposed in Reference 2. The S_T component in (b) is different from the Si1+ suboxide component. The relative intensity of S_T is approximately the same as the sum of the relative intensities of the *S*, *SS*, *C*, and *S*' components in (a).

Figure 5. (Color online.) Si 2*p* spectrum obtained with 260 eV photons. The energy shift and Gaussian width of the peaks employed for the fit are those from Reference 28. The extra component, S_T, was not considered in the series of works by Himpsel et al. 28 However, as shown in the inset, the fit is improved in the circled region by including S_T.

Figure 6. (Color online.) Fit of the Si 2*p* spectra from Si (001) annealed at 800 °C for 16 second; the data was acquired at 35° take-off angle (from the surface). a) Fit employing the α and β components proposed by Oh et al. 29. b) Fit employing the S_T component proposed in this work. This shows that the component β is not required to obtain a good 16 fit.

Figure 7. (Color online.) Correlation between the Si^{4+} shift and the thickness of the S_T layer. a) Dependence of the Si^{4+} shift and the thickness of the S_T layer. b) The blue dashed line corresponds to the fit in which it is considers that the surface charge is constant. The solid cardinal line corresponds the fit to the model presented in this paper (described in the text) in which the surface charge varies with the thickness of the S_T layer. In contrast with the constant layer model, our model reproduces the jump on the binding energy of the Si 2*p* peak in Si^{+4} between the 75 s and 900 °C samples.

Journal of Vacuum Science & Technology A

PLEASE CITE THIS ARTICLE AS DOI: 10.1116/6.0002690

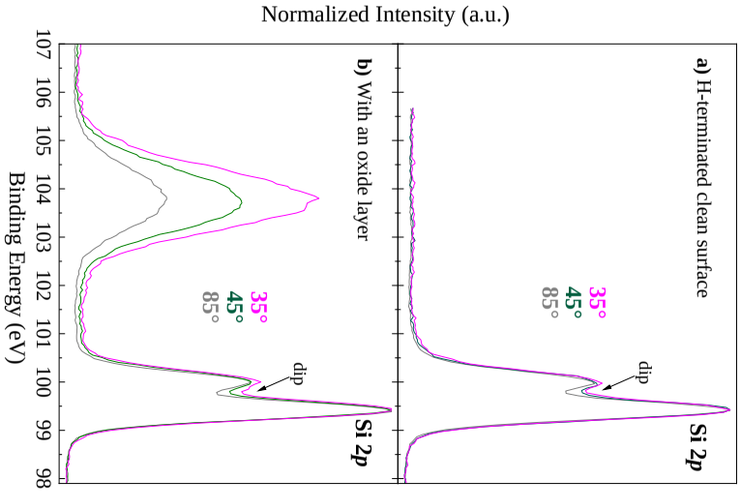

Journal of Vacuum Science & Technology A

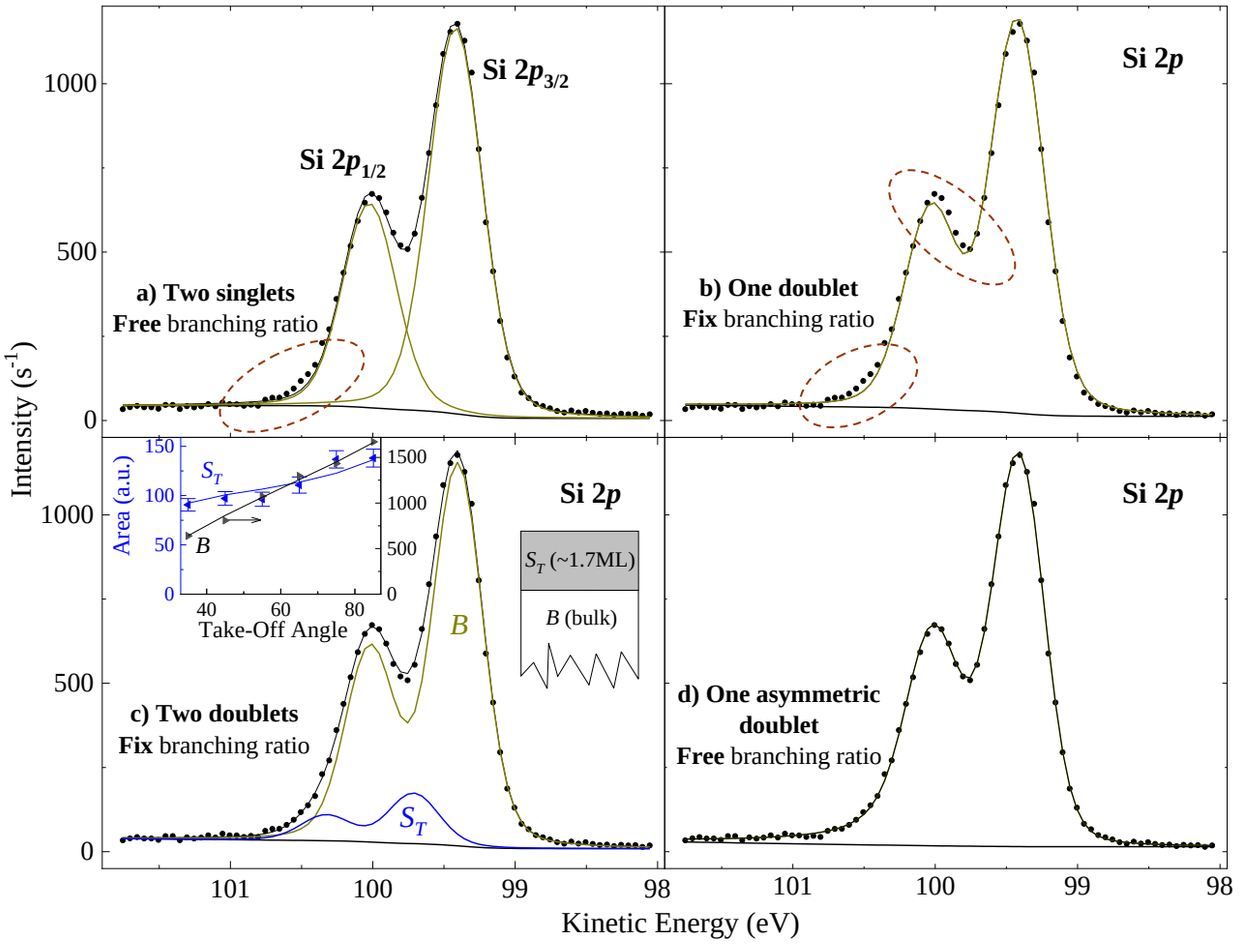

Journal of Vacuum Science & Technology A

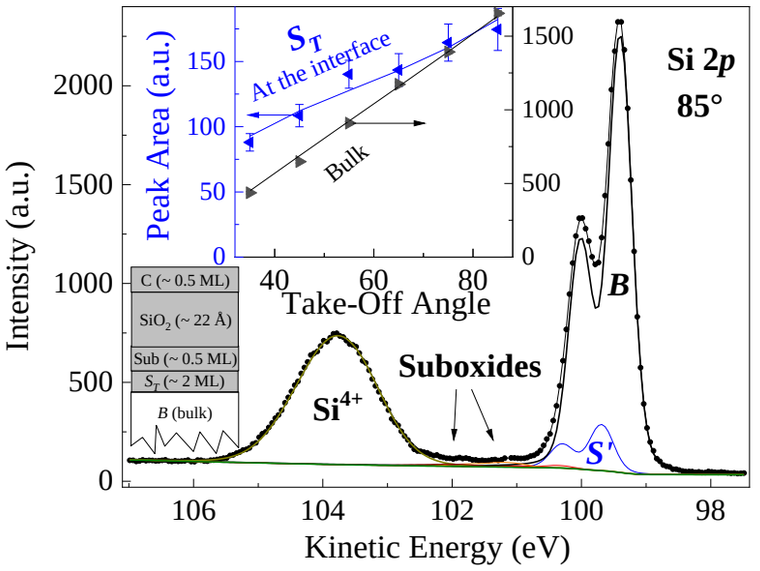

Journal of Vacuum Science & Technology A

PLEASE CITE THIS ARTICLE AS DOI: 10.1116/6.0002690

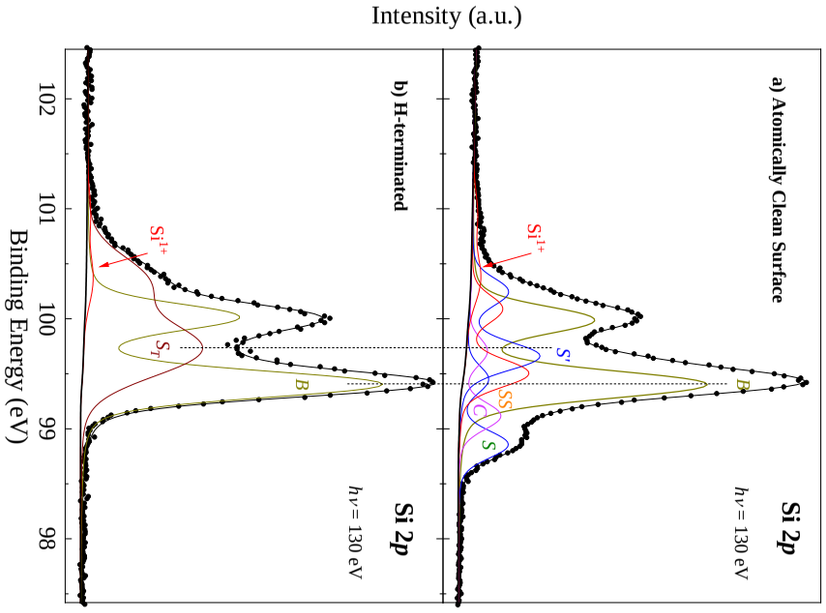

Journal of Vacuum Science & Technology A

PLEASE CITE THIS ARTICLE AS DOI: 10.1116/6.0002690

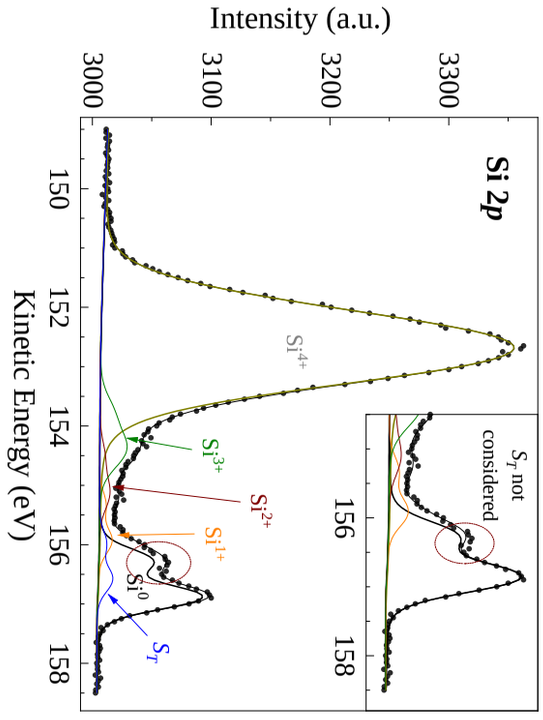

Journal of Vacuum Science & Technology A

PLEASE CITE THIS ARTICLE AS DOI: 10.1116/6.0002690